CHAPTER 58

TSUNAMI PROPAGATION IN THE PACIFIC OCEAN

by

Manfred Engel[+] and Wilfried Zahel[++]

ABSTRACT

The Alaska tsunami of March 28, 1964, caused by a tectonic up-
lift, propagated across the Pacific Ocean and was even recor-
ded at the shores of New Zealand and the Antarctica. The large
distance propagation of this tsunami is investigated by a nu-
merical model based on the shallow water equations. The model
includes bottom friction, eddy viscosity and Coriolis accele-
ration and yields the water elevation and the vertically inte-
grated current velocity. The generation mechanism is given by
a simplified initial condition, that is derived from the obser-
ved average uplift of 1.8 m for an area of 110000 km^2 on the
Continental Shelf. The computed tsunami propagation is presen-
ted by means of the first wave travel time and height on Paci-
fic Ocean maps and by giving sea surface time series for selec-
ted stations. These computed results are compared with obser-
vations, especially considering the limitations of the model due
to the coarse grid net having been used.

INTRODUCTION

Research of tsunami hydrodynamics until now seems to be split
up into three parts: generation mechanisms, propagation of tsu-
namis in open ocean, amplification and run up at coasts. A great
variety of methods is used for these investigations, such as
model building on the basis of analytical or numerical soluti-
ons to the hydrodynamic equations and carrying out experiments
with hydraulic models of the prototypes.

The present contribution shall be understood as an attempt to
simulate the open ocean propagation of an actual tsunami by hy-
drodynamic-numerical modelling considering as many physical
properties as possible. Use was made of a 1°-World-Ocean-mo-
del, that yielded realistic results when it was applied to the
computation of oceanic tides by ZAHEL, 1975. Because of the far
smaller characteristic wave lengths of tsunamis, some preinvesti-
gations had to be performed in order to throw light upon the
question, whether the grid net resolution suffices to comprehend
the main features of tsunami propagation and initiation. Refer-
ence will be made to these considerations in the Chapter PREIN-
VESTIGATIONS.

The 1964 Alaska tsunami was characterized by an extended uplif-
ted area with an average sea surface elevation of 1.8 m and by

---

+ Institut für Meereskunde, Universität Hamburg
++ do.

a period of about 1.3 hours of the radiated wave (BERG et al., 1972). Because of these relatively proper conditions for the application of the available model we decided to simulate this actual tsunami. A description of the model is given in the Chapter THE HYDRODYNAMIC MODEL, the grid net arrangement and the numerical treatment of the differential equations are out-lined there.

The Chapter COMPUTATIONAL RESULTS contains a discussion of the computational results in view of observations. The distributi-ons of propagation times and heights of the first crest are presented on Pacific Ocean maps, time series of the surface elevation are given for selected positions being as near as possible to gauge positions and originating from all over the Pacific Ocean.

PREINVESTIGATIONS

In order to get an insight into the problems of a large scale numerical tsunami propagation model, we first ran some one-di-mensional models. Especially the usefulness of a 110km-grid-resolution with respect to the propagation of the main wave train had to be investigated. As already can be seen from the dispersion relation yielded by the explicit difference equation scheme, the phase velocity for waves with periods longer than 1.3 hours, a value which was observed in connection with the Alaska tsunami, is only insignificantly falsified by the appli-ed numerical treatment in deep ocean areas. Also the decay time due to eddy viscosity remains proportional to the square of the wavelength and to the inverse eddy coefficient for such long period waves in the numerical procedure, so they are insignifi-cantly affected by eddy viscosity while propagating across the Pacific Ocean. Because of the exclusion of small scale proces-ses in the model the convective terms were neglected. A simple shelf radiation model, allowing no reflection to take place at the right hand side open boundary, gave a good impression of the continous energy radiation from the shelf area for a given initial water elevation distribution (Fig.1). This distributi-on was well resolved by the used grid net with a spatial grid point distance of 7.4 km. Against that the global model is far from being able to take care of a realistic generation mecha-nism, only the estimated potential energy of the realistic up-lift in the generation region could be considered.

In a $1^{\circ} \times 2^{\circ}$-testing-model two different schematic distributions of the uplift with the same potential energy content were pre-scribed, one with different uplifts,the other with a uniform uplift at the eight marked grid points. Fig.2 shows the travel times of the first wave crest for both tsunamis thus having been initiated, that means there is no difference appearing within the accuracy of the plot. Because of this conformity in travel times we finally ran the global model for the Alaska tsunami with the simplest generation mechanism, a uniform ini-tial surface elevation of 2 m at these grid points, the initi-al potential energy amounting to 2.0 X 10^{22} erg by this way.
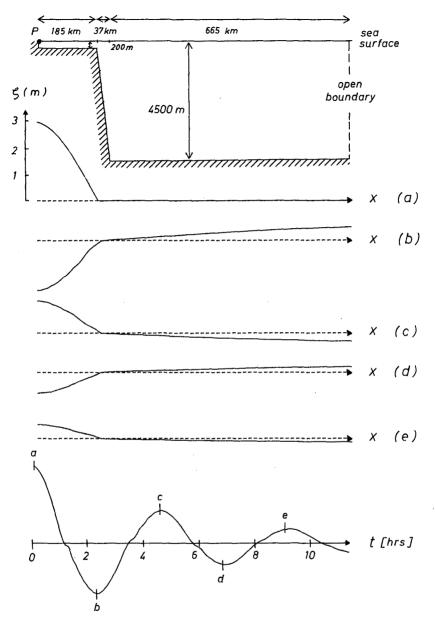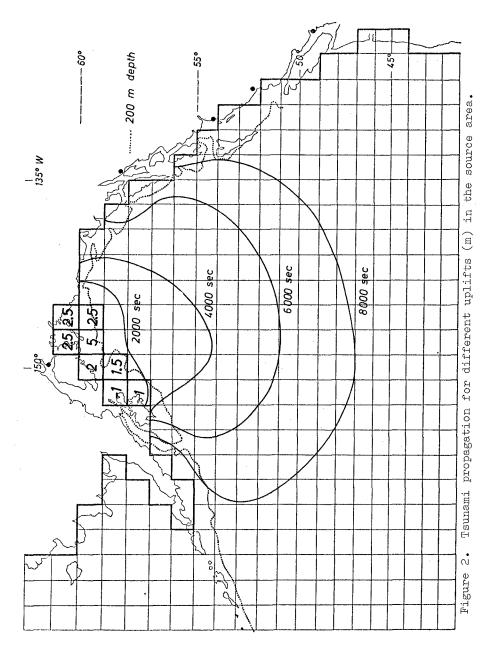
Figure 1. Distribution of sea surface elevations in space and time(at Point P) for computed wave radiation from an idealized shelf.

Figure 2. Tsunami propagation for different uplifts (m) in the source area.

THE HYDRODYNAMIC MODEL

The model has already been used for ocean tide investigations by ZAHEL,1975 and it was developed from that one presented by ZAHEL,1970 in detail.The equations of motion for long waves and the equation of continuity are taken as a basis for the model. With t=time, λ=geographic longitude, φ=geographic latitude they are given by :

$$\frac{\partial u}{\partial t} - 2\omega\sin\varphi\, v + \frac{r(u^2+v^2)^{1/2}}{D}\, u + R_\lambda + \frac{g}{R\cos\varphi}\frac{\partial \zeta}{\partial \lambda} = 0$$

$$\frac{\partial v}{\partial t} + 2\omega\sin\varphi\, u + \frac{r(u^2+v^2)^{1/2}}{D}\, v + R_\varphi + \frac{g}{R}\frac{\partial \zeta}{\partial \varphi} = 0$$

$$\frac{\partial \zeta}{\partial t} + \frac{1}{R\cos\varphi}\left(\frac{\partial(Du)}{\partial \lambda} + \frac{\partial(Dv\cos\varphi)}{\partial \varphi}\right) = 0$$

$u=u(\lambda,\varphi)$, $v=v(\lambda,\varphi)$ denote the vertically integrated current velocity components, eastward and westward respectively, $D = d+\zeta$ the actual depth and $\zeta = \zeta(\lambda,\varphi)$ the surface displacement. The lateral eddy viscosity terms

$$R_\lambda = A_h \Delta u + A_h R^{-2}(- u(1+tg^2\varphi) - 2\frac{tg\varphi}{\cos\varphi}\frac{\partial v}{\partial \lambda})$$

$$R_\varphi = A_h \Delta v + A_h R^{-2}(- v(1+tg^2\varphi) + 2\frac{tg\varphi}{\cos\varphi}\frac{\partial u}{\partial \lambda}) \quad \text{roughly take}$$

account of turbulence effects on the mean flow. A_h is a constant coefficient, $A_h = 10^5$ m^2/sec is assumed in this case.

As the model is a global one, the domain of integration of the differential equations is only bounded by coasts, which are defined to be impermeable. Therefore the normal component of the current velocity is assumed to be zero at the boundary. Provided that proper initial conditions are prescribed, this condition uniquely determines the solution of the first order equation system. The inclusion of the second order term requires the further homogeneous boundary condition of zero current velocity. The initial conditions defining the tsunami generation mechanism, in strong simplification are given by an uplift distribution of the sea level and zero current velocity at t = 0.

Although in the present problem the polar regions are unimportant, the numerical procedure shall for completeness briefly be described as it is applied to the world ocean as a whole. In order to avoid a strong reduction of the grid-point-distance due to the convergence of meridians, poleward doubling of the zonal angular grid-point-distance is performed at five parallels, namely at 55°N, 55°S, 72°N, 72°S, 81°N. Hence the grid net covering the globe is characterized by a mesh size of 1°X1° between 55°N and 55°S, of 1°X2° between 55°N and 72°N as well as between 55°S and 72°S, of 1°X4° southward of 72°S as well as between 72°N and 81°N. Finally, northward of 81°N adjacent grid points are 1° distant on a meridian and 8° distant on a parallel, respectively. The parallels defining the mentioned transitions are marked on Fig.3, which shows the approximated coastlines and the bottom topography that is used in the model.

The numerical scheme has been used in the following form :

$$D_+^t u_{i,j}^n - 2\omega \sin\varphi_i \; \bar{v}_{i,j}^n + \frac{r\sqrt{(u_{i,j}^n)^2+(\bar{v}_{i,j}^n)^2}}{\bar{D}_{i,j}^n} \; u_{i,j}^n + (R\lambda)_{i,j}^n +$$

$$+ \frac{g}{R\,\cos\varphi_i} \left(D_o^\lambda \zeta_{i,j}^n \; a(\varphi_i) + D_o^\lambda \zeta_{i,j}^{n+1} \cdot b(\varphi_i) \right) = 0$$

$$i=1,3,5,7,\ldots \; ; \; j=1,3,5,7,\ldots$$

$$D_+^t v_{i,j}^n + 2\omega \sin\varphi_i \; \bar{u}_{i,j}^n + \frac{r\sqrt{(\bar{u}_{i,j}^n)^2+(v_{i,j}^n)^2}}{\bar{D}_{i,j}^n} \; v_{i,j}^n + (R\varphi)_{i,j}^n +$$

$$+ \frac{g}{R} \left(D_o^\varphi \zeta_{i,j}^n \right) = 0 \qquad i=0,2,4,6,\ldots \; ; \; j=0,2,4,6,\ldots$$

$$D_+^t \zeta_{i,j}^n + \frac{1}{R\,\cos\varphi_i}\left(D_o^\lambda (\bar{D}_{i,j}^n \; u_{i,j}^{n+1}) + D_o^\varphi (\bar{D}_{i,j}^n \cdot v_{i,j}^{n+1} \cos\varphi_i) \right) = 0$$

$$i=1,3,5,7,\ldots \; ; \; j=0,2,4,6,\ldots$$

$$D_+^t w := \frac{w(t+\Delta t)-w(t)}{\Delta t} \; ; \quad D_o^\Psi w := \frac{w(\Psi+\Delta\Psi/2)-w(\Psi-\Delta\Psi/2)}{\Delta\Psi} \quad \Psi = \lambda, \varphi;$$

$$w_{i,j}^n := w(i\cdot\Delta\varphi/2, j\cdot\Delta\lambda/2, n\cdot\Delta t) \quad w=\zeta, \; u, \; v \; ; \quad a(\varphi_i)+b(\varphi_i)=1$$

$0 \le a \le 1, \; 0 \le b \le 1$. Except from a small neighbourhood of the North Pole a=1, b=0 is taken. Thus the applied time stepping scheme is explicit in the area of tsunami propagation in question. The only transition from one uniform grid net to another in this area takes place at 55°N. Because of technical reasons arrival times and surface elevations of the first maximum were only stored for the 1°X1° area and for the Gulf of Alaska separately, so that this information was lost for the Bering Sea north of 55°N, as can be seen on Fig.5 and Fig.10.

To give an impression what global results gained by this 1°-model look like, amplitudes and phases of the rather well reproduced M_2-tide are presented on Fig.4, which is taken from ZAHEL, 1975. [2] When computing tsunami propagation, calculations are, of course, not performed for areas where the tsunami will not get in the time of interest.

The same hydrodynamic method was applied by ENGEL,1974 to tsunami simulation in the Black Sea.

Figure 3. Depth distribution and boundaries as used in the 1°-World-Ocean-model. Lines of equal depth given for 200m (1), 2000m (2), 3000m (3), 4000m (4) and 5000m (5). Northern and southern hemisphere in stereographic projection.
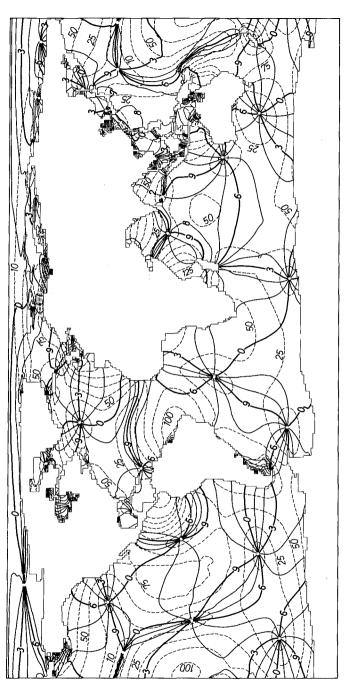
1°-OCEAN-MODEL
M_2-Tide

cotidal lines (—) and corange lines (---)

phases in lunar hours referred to meridian passage at Greenwich

amplitudes in centimetres (10, 25, 50, 75, 100, 125, 150, 200)

Figure 4.

COMPUTATIONAL RESULTS

To give an idea of computed tsunami propagation properties we at first refer to the propagation time of the first maximum. The isolines of this time, that can better be defined than the arrival time of the first disturbance, are displayed on Fig.5. Due to the applied simple generation mechanism even the tsunami propagating in the open ocean will differ from the real one when being computed by the 1°-model. This fact gets obvious when considering e.g. the slow ascent of the computed water level compared with the real one at certain oceanic islands. Nevertheless, it is expected from the computations, having been carried out on the basis of a hydrodynamic model, that the characteristic features of the radiated long wave are yielded concerning its propagation in the open ocean. In order to give an impression of the effects of depth distribution on the wave propagation, the lines of equal depth have been entered into the presentation. There are obvious features as to the deformation of travel time isolines due to the bottom topography as e.g. the high speed propagation in the central South Pacific and the comparatively delayed propagation through the shallower parts of the south-eastern Pacific. Refraction effects gathered from Fig.5 at the transition zone from the open ocean to the American coast are evidently not realistic in all cases because of the poor resolution of the narrow shelf there. An improvement of the results,concerning phenomena that arise on small scale areas,could be obtained by including nested grids into· the global one. A very distinct effect due to reflection can be recognized at the Japan Trench as well as at the Kuril Trench. While the reflected wave contributes to the formation of the first maximum, superposition with the arriving second wave takes place before the first one has reached its maximum, and in this way the particular propagation pattern comes about. Other effects of reflection cannot be detected from the presentation of the first maximum, although, of course, being fully inherent in this model.

Before comparing computed arrival times with gauge observations, some limitations of the model shall be summarized. As the wave generation was performed rather schematically, the computed wave train only reflects the gross features of the shelf source area and the initial condition in sea level variation and current velocity and therefore it cannot be considered to be directly comparable with the real one. The phase velocity in any numerical model is subject to discretization errors depending on the difference scheme, on the grid resolution and on the wave length governing the physical process being modelled. The described 1°-model admits long waves with at least thousand kilometers wavelength to propagate in the deep ocean with a phase velocity deviating less than 1 per cent in magnitude from the real phase velocity. A somehow generated wave train containing a broad spectrum of wave lengths will at all events be dispersed numerically. The leading wave of the investigated Alaska tsunami, characterized by a period of 1.3 hours, thus proves to be long enough in deep water to be subject to an appropriate approximation concerning the phase velocity. On extended shelf areas, like that of the Yellow Sea, the computed wave properties are unreliable because of numerical dispersion effects.

Moreover the poor resolution of shelf areas extending in front
of coasts leads to insufficient approximation of the wave ar-
riving at the coast, since gauge records coming from such co-
asts are characterized by the response behaviour to the local
topography. As the most available gauge records refer to such
positions,computed and observed values can also for this rea-
son not directly be compared.

The positions for which the water elevations have been printed
out for every time step are marked on Fig.6, they are close to
places where gauge data were gained. Fig.7 and Fig.8 show the
computed water elevations at these locations, with the arrival
time of a significant disturbance,defined by a water level ri-
se of 2 mm and indicated by the beginning of the curves. The
longer vertical lines represent observed arrival times, taken
from the gauge records published by SPAETH and BERKMAN,1967
and others. The above remarks are applicable to the comparison
at the mentioned positions, showing itself by the fact that
opposite to the observations the computed water elevations
yield similar curves for all stations. There is an almost con-
stant time difference between the computed first disturbance
and the first wave crest, it amounts to about 65 minutes. Hen-
ce, taking this first disturbance instead of the first wave
maximum when representing tsunami propagation, a picture of
high similarity to that one given on Fig.5 would result. In
all cases the observed arrival time is later than the computed
one, the difference running up to about 10 minutes except for
Galapagos and Lyttelton, where it is nearly 3 times larger.
The relatively large time difference at Galapagos may result
from the fact that the gauge position at San Cristobal is lo-
cated farther from the source area than the nearest grid point,
which moreover lies on the other side of the island. Because
of its backward position in a bight there are similar diffi-
culties in adjoining a grid point to Lyttelton. Finally, it
proves to be difficult to recognize a 2 mm disturbance on a
gauge record in any case.

Three N–S–surface profiles are plotted on Fig.9, beginning in
the source area and extending southward as far as the wave has
propagated. As can be seen also from this picture, the form of
the leading wave is preserved, although its energy decreases
successively. To get an idea of the spatial energy supply, re-
ference to at least the surface elevations shall be made. Fig.
10 shows the computed surface elevation of the first wave ma-
ximum in mm. Effects of bottom topography can easily be recog-
nized,e.g. regarding the increased magnitude of elevations at
the Hawaiian Ridge, at the north-east coast of Australia and
at the American coast. Obviously these surface elevations are
not suitable for being compared with the observed ones, they
at best can be hoped to be a first approximation for the wave
entering coastal areas.

Thus applying the global hydrodynamic model to the 1964 Alaska
tsunami is understood as a first step in trying to bridge the
gap between investigations concerned with generation mechanisms
and those studying run up processes. No model can explicitly
include all physical processes governing tsunamis, and therefore
besides the application of nesting techniques parameterizations

of significant processes will have to be introduced, in order
to achieve an overlapping modelling of generation, propagati-
on and run up of tsunamis that will be of use for practical
purposes.

REFERENCES

BERG, E. et al., Source of the Major Tsunami, Contributions
of the Hawaii Institute of Geophysics, University of Hawaii,
No. 310, 1972

ENGEL, M., Hydrodynamisch-numerische Ermittlung von Bewegungs-
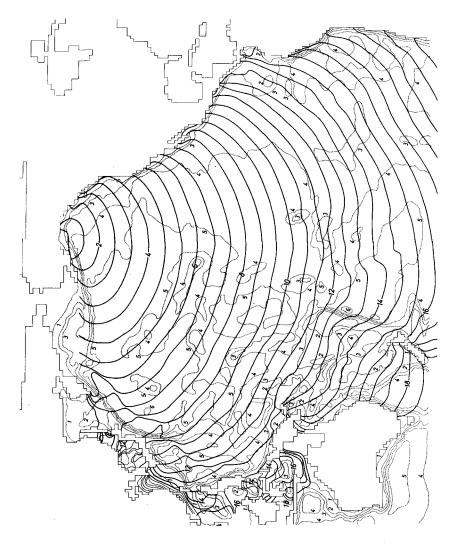vorgängen im Schwarzen Meer, Mitt. d. Inst. f. Meereskd. der
Univ. Hamburg, XXII, 1974

SPAETH, M.G., and S.C. BERKMAN, The tsunami of March 28,1964 ,
as recorded at tide stations, Environmental Science Services
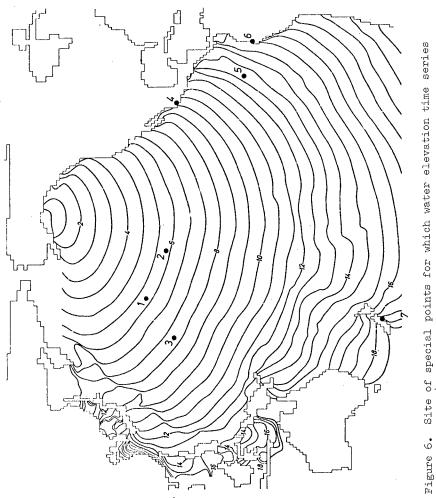Administration Technical Report C&GS 33, 1967

ZAHEL, W., Die Reproduktion gezeitenbedingter Bewegungsvorgän-
ge im Weltozean mittels des hydrodynamisch-numerischen Ver-
fahrens, Mitt. d. Inst. f. Meereskd. der Univ. Hamburg, XVII,
1970

ZAHEL, W., Mathematical and Physical Characteristics and Re-
cent Results of Ocean Tide Models, Proceedings of the IRIA In-
ternational Colloquium on Numerical Methods of Scientific and
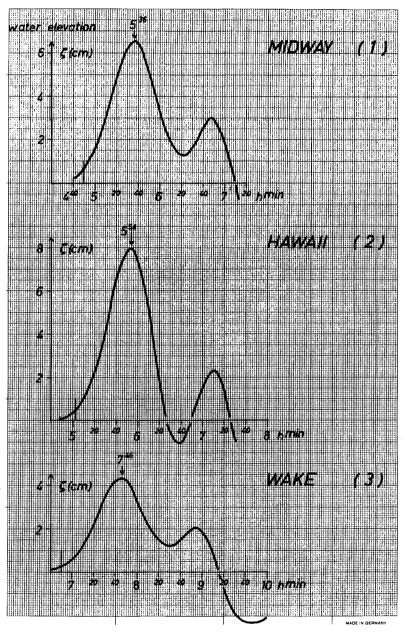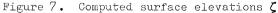Technical Computation, December 1975, Lecture Notes in Mathe-
matics (in press)

Figure 5.   Computed propagation of the 1964 Alaska tsunami.
Full line ──2── propagation time of first wave
crest in hours.
Dotted line ••••2•••• depth isoline with 1: 200m ,
2: 2000m, 3: 3000m, 4: 4000m, 5: 5000m .

Figure 6. Site of special points for which water elevation time series are given
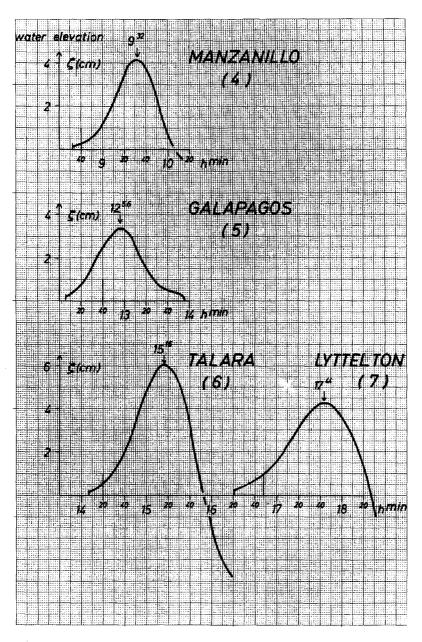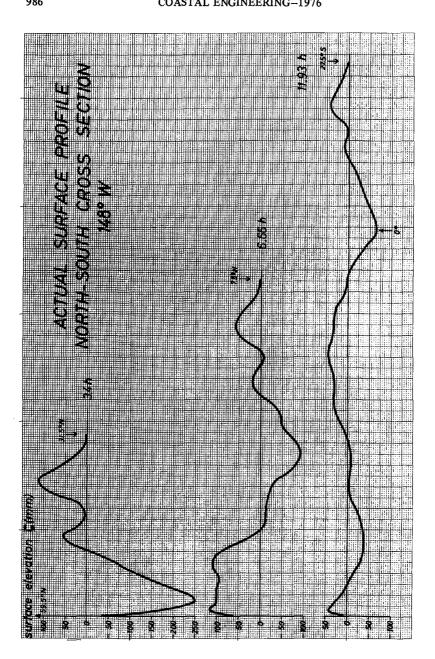
Figure 7. Computed surface elevations ζ
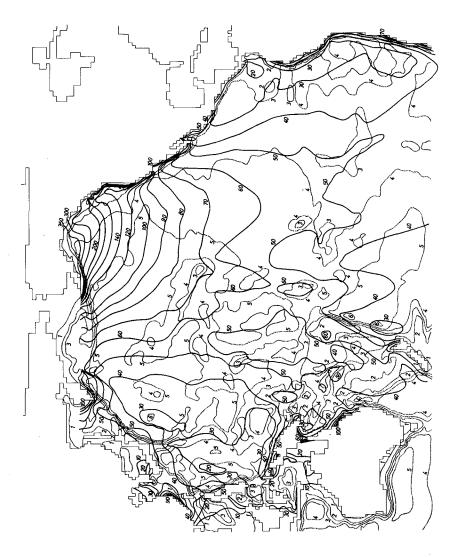
Figure 8. Computed surface elevations ζ

Figure 9.

Figure 10. Computed propagation of the 1964 Alaska tsunami.
Full line——40—— surface elevation of the first wave ma-
ximum in mm.   4
Dotted line .... depth isoline with 1: 200m, 2: 2000m,
3: 3000m, 4: 4000m, 5: 5000m, 6: 6000m .